Computers and Electronics in Agriculture 79 (2011) 159–168

Contents lists available at SciVerse ScienceDirect

Computers and Electronics in Agriculture

journal homepage: www.elsevier.com/locate/compag

Line-scan hyperspectral imaging system for real-time inspection of poultry carcasses with fecal material and ingesta

Seung Chul Yoon *, Bosoon Park, Kurt C. Lawrence, William R. Windham, Gerald W. Heitschmidt

US Department of Agriculture, Agricultural Research Service, Richard Russell Research Center, 950 College Station Rd., Athens, GA 30605, USA

ARTICLE INFO

Article history:
Received 1 November 2010
Received in revised form 22 August 2011
Accepted 16 September 2011

Keywords:
Real-time multispectral imaging
Hyperspectral imaging
Line scan
Poultry processing
Food safety
Fecal detection

ABSTRACT

In poultry processing plants, fecal material and ingesta are the primary source of carcass contamination with microbial pathogens. The current practice of the poultry inspection in the United States is primarily human visual observations. Since the visual inspection is becoming more challenging in poultry processing plants adopting high-speed lines, a rapid sorting system could significantly improve the detection and monitoring of carcasses with surface fecal material and ingesta. As a result, we developed a prototype line-scan hyperspectral imaging system configured as a real-time multispectral imaging subsystem for online detection of surface fecal material and ingesta. Specifically, we integrated a commercially available off-the-shelf hyperspectral image camera into the system with two line lights and a custom software program for real-time multispectral imaging. The bottleneck of the imaging system was the data acquisition. For that reason, a multithreaded software architecture was designed and implemented not only to meet the application requirements such as speed and detection accuracy, but also to be customizable to different imaging applications such as systemic disease detection in the future. The image acquisition and processing speed tests confirmed the system could operate to scan poultry carcasses in commercial poultry processing plants. The fecal detection algorithm was based on the previous research using different hyperspectral imaging systems. A new carcass detection and image formation algorithm was developed to allow existing image processing and detection algorithms reusable without any modifications. Sixteen chicken carcasses and four different types of fecal and ingesta samples were used in a study to test the imaging system at two different speeds (140 birds per minute and 180 birds per minute) in a pilot-scale poultry processing facility. The study found that the system could grab and process three waveband images of carcasses moving up to 180 birds per minute (a line-scan rate 286 Hz) and detect fecal material and ingesta on their surfaces. The detection accuracy of the system varied between 89% and 98% with minimum false positive errors (less than 1%), depending on tested detection algorithms. Therefore, these findings provide the basis of not only a commercially viable imaging platform for fecal detection but also a single poultry inspection system for multiple tasks such as systemic disease detection and quality sorting.

Published by Elsevier B.V.

1. Introduction

Multispectral imaging is a popular and viable solution for many online sorting applications. However, the development of a dedicated real-time multispectral imaging system is not trivial. In fact, challenges faced by a real-time imaging system designer come from both hardware and software issues (Kehtarnavaz and Gamadia, 2006). From the hardware point of view, a challenge is to determine whether a given hardware platform can produce the data with quality and quantity required by an application in real-time deadlines. From the software point of view, a challenge involved is to implement algorithms developed in non real-time computing environments such as hyperspectral imaging into a real time version. Therefore, the development of a real-time spectral imaging system for online sorting is still largely out of reach for many researchers in the field of agriculture and food.

Hyperspectral imaging has great potential as a non-destructive measurement tool for safety inspection and quality control of agricultural and food products. However, problems such as high costs and difficulties with high-speed data acquisition and process have so far limited the use of hyperspectral imaging largely to a research tool for developing separate multispectral imaging techniques and systems. The difficulties largely stem from the 3D data-cube formation process of the hyperspectral imaging technology scanning a scene with a 2D area detector over time to acquire the third dimension of data. Nonetheless, line-scan near-infrared (NIR) hyperspectral imagers were utilized for high-speed industrial

* Corresponding author.
E-mail address: seungchul.yoon@ars.usda.gov (S.C. Yoon).

0168-1699/$ - see front matter Published by Elsevier B.V.
doi:10.1016/j.compag.2011.09.008

polymer sorting (Leitner et al., 2003) and cellulose-based material sorting (Tatzer et al., 2005). However, these online imaging applications were feasible mainly because a CMOS readout integrated circuit (ROIC) was used for the NIR cameras with InGaAs sensors (Grietens, 2009). CMOS ROIC provides faster pixel-readout rates than conventional CCD circuits (Litwiller, 2001, 2005). However, silicon-based CCD sensors are still predominantly adopted for high-quality hyperspectral image cameras covering the visible and near-infrared (VNIR) spectral range of 400–1000 nm. For that reason, real-time imaging with a line-scan VNIR hyperspectral imager did not get much attention until recently when researchers recognized the non-contiguous partial readout capability of the electron-multiplying CCD (EMCCD). This capability implied that only a few discrete wavelengths could be selected by the user for a rapid readout with a small amount of data. As a result, a multispectral imaging mode could be configured using a line-scan VNIR hyperspectral imager with EMCCD. Based on this idea, line-scan VNIR hyperspectral cameras were used for online apple sorting (Kim et al., 2008) and unwholesome poultry-carcass sorting (Chao et al., 2007, 2008). More recently, a study demonstrated the feasibility of a line-scan VNIR imager with EMCCD for detecting fecal material and ingesta on poultry carcasses, but not in real-time (Park et al., 2011). Thus, a systematic study for design and implementation of a real-time imaging system for online fecal detection would be still necessary. Also, there was a need for a fast algorithm to form an image corresponding to an individual chicken carcass from line scan data in order to minimize the complexity of the image processing algorithms that were developed with 2D images not 1D line data.

In the US poultry processing plants under USDA inspection, all carcasses are subject to post-mortem inspection due to food safety concerns. Particularly, fecal contamination and infectious conditions like systemic disease are considered important post-mortem food safety hazards because they may harbor foodborne pathogens and other infectious agents (FSIS, 1998a,b, 2004). Currently, USDA inspectors visually monitor poultry carcasses for detecting surface fecal materials (interchangeably with fecal and ingesta material in this paper) and infectious conditions. However, human visual inspection is labor-intensive and inevitably prone to human subjectivity and variability. In addition, in US plants operating high-speed shackle lines at 140–180 birds per minute (bpm), visual inspection is becoming more challenging because more USDA inspectors and plant helpers are needed to meet the throughput increase. Especially for fecal detection, a small amount of fecal material (ceca, colon, and duodenum) and ingesta (ingested matter) are very difficult to detect by naked eyes from fast moving carcasses with consistent performance over long time.

Previously, a spectroscopic study found reflectance characteristics of fecal material and ingesta were different from them of normal carcass features like skin, meat and blood spots (Windham et al., 2003a,b). This difference in spectral characteristics led to develop several fecal detection technologies based on either hyperspectral imaging (Park et al., 2002; Lawrence et al., 2003a) or multispectral imaging (Park et al., 2004, 2007; Yoon et al., 2007, 2010). The best performing algorithm for fecal detection was an algorithm using a band ratio of 517- and 565-nm wavebands and another band ratio of 517- and 802-nm wavebands followed by thresholding (Park et al., 2002; Windham et al., 2003b; Heitschmidt et al., 2007). From the hyperspectral research findings, a multispectral imaging system using a conventional CCD camera with optical trim filters was developed for online fecal detection (Park et al., 2004). However, a filter-based multispectral imager was not customizable to be used in different applications. Therefore, the objectives of this research were to develop a general-purpose line-scan VNIR hyperspectral imaging system, configure it as a real-time multispectral imaging system, apply it for online sorting of poultry carcasses contaminated by fecal material and ingesta, and evaluate it.

2. Methods and materials

2.1. Hyperspectral imaging system: hardware

The hardware of the hyperspectral imaging system consisted of a line-scan hyperspectral camera, two pairs of light sources, power supplies, a computer, and a portable platform. The hyperspectral camera consisted of an imaging spectrograph (HyperSpec VNIR, Headwall Photonics, Fitchburg, MA, USA), an EMCCD sensor (Luca-R, Andor Technology, Belfast, UK) and an objective lens (CNG f-1.4/12 mm, Schneider Optics, Hauppauge, NY, USA). The spectral range, slit-width, and spectral resolution of the imaging spectrograph were 400–1000 nm, 40-μm and 4 nm, respectively. The EMCCD sensor was a USB2.0 monochrome camera with 14 bits and 1004×1002 pixels, and thermoelectrically cooled (−20 °C). The full frame rate was 12.4 Hz. The pixel readout rate was 13.5 MHz. The objective lens mounted to the spectrograph's entrance slit was a compact C-mount lens with 12-mm focal length. The position and orientation of the hyperspectral camera were adjusted by trial and error in order to minimize shape distortions caused by misaligned line scanning and also to match up with the detector orientation. The detector orientation was determined by choosing the pixel dimensions of 1004×1002 pixels to be the spatial and spectral dimensions, respectively. An industrial portable computer (SAX 903, ACME Portable Machines, Inc., Azusa, CA, USA) was used for camera control and software operation. The computer was equipped with an Intel's Xeon CPU (2.8 GHz) and a 3.0 GB RAM. The operating system was Microsoft Windows XP Professional SP3. The system was equipped with two pairs of different line illuminators but only a pair of tungsten–halogen line lights was tested in this research. The other pair was white LED line lights (Fig. 1). The inter-distance of two tungsten–halogen line lights was 29 cm when used. Each tungsten–halogen light source consisted of a 150-W fiber optic line illuminator (Fiber Lite A-240L and A-240P, Dolan-Jenner Industries, Boxborough, MA, USA) with a focusing lens.

2.2. Application requirements analysis

2.2.1. Line scan resolution and rate

In 140-bpm processing lines, the maximum time allowed to complete data acquisition and processing is about 0.4 s (428.47 ms) per bird. The inter-distance between adjacent shackles was 15.24 cm (6 in.). The minimum amount of fecal contaminants harmful enough to humans was as little as 5 mg (Berrang et al., 2004). The average sample size of a 5-mg spot was approximately 10 mm^2 that was the minimum sample size to resolve by the fecal detection system. The working distance from the 12-mm objective lens to the shackle line was 0.4826-m (19-in.) that ensured the full scan of a carcass from top to bottom. The field of view (FOV) along the scan line was approximately 32 cm. The instantaneous field of view (IFOV) across the scan line was approximately 1.6 mm. The instantaneous scan size on a flat surface placed at the working distance was a narrow rectangle of 1.6 mm (W) × 32 cm (H). Hence, in theory, each square pixel on the EMCCD detector was mapped to an area of 1.6 mm (W) × 0.3 mm (H) that was the minimum scan size. Therefore, the minimum scan area of each pixel was 0.48 mm^2. However, this calculation did not consider a motion factor that may cause undersampling. The minimum scanning rate to fully image a moving bird without undersampling was 95 scans per bird at 140 bpm (from 15.24 cm/1.6 mm). If undersampling, i.e. excessive skipping, happens, it is more likely to miss small

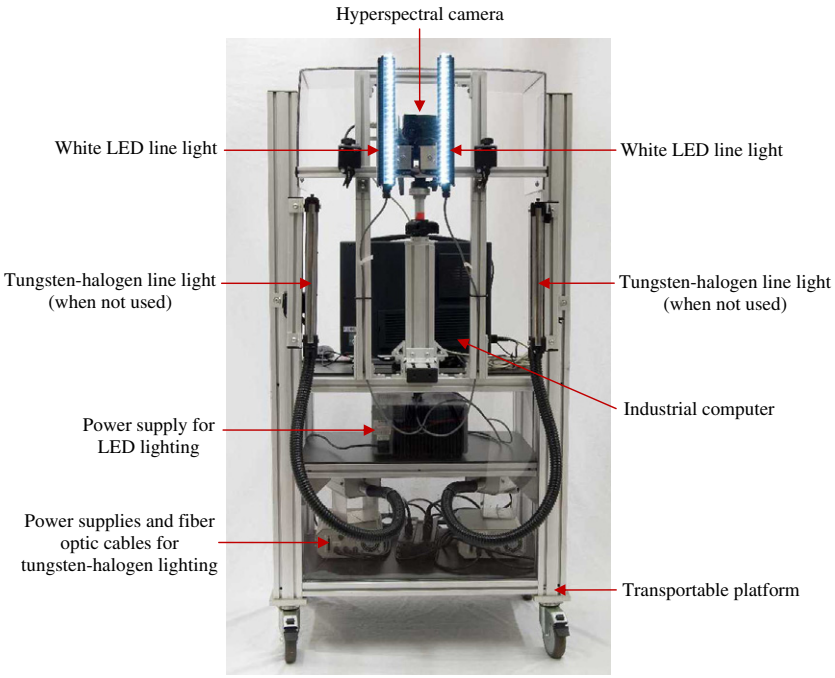

Fig. 1. Overview of the hyperspectral imaging system.

feces. In practice, oversampling will increase a spatial resolution along the motion direction and thus recommended. A rule of thumb is to add 25% more lines (119 lines in this case). Therefore, the system was designed and tested to meet this line-scan rate requirement (95–119 line scans per bird) by using shorter exposure time, image binning, fast image processing algorithm and multitasking.

2.2.2. Data reduction for fast data transfer

It is desirable to reduce exposure time in order to minimize the image blur caused by shackle motions during the CCD exposure time. In theory, exposure times of 1–3 ms may cover scan areas of 0.59–0.8 mm^2 that are much smaller than the minimum sample area 10 mm^2. However, the degree of motion blurring as function of exposure time is still unknown. The frame transfer mode of the CCD was used to ensure no delay between successive exposures. Without the frame transfer mode, pixel read-out time would become delay time in between exposures. When 95 lines are obtained per bird at 140 bpm, the processing time per line is 4.5 ms (equivalently, 222 scan lines/s). Hence, the frame rate should be at least 222 Hz to avoid system malfunctions. Image binning was a key technique to achieve the desired frame rate. The spatial dimension was binned down to the half resolution with 502 pixels. The spectral dimension was binned only at three pre-defined non-contiguous bands (called random tracks) centered at 517, 565 and 802 nm for this research. After binning, the spectral image resolution became 3 (spectral) × 502 (spatial) per scan. After padding 10 dummy zeros to the spatial resolution for the sake of easy programming, the dimension of the final hyperspectral data cube became N (width) × 512 (height) × 3 (spectral bands) pixels, where N was the number of line scans per bird (about 95–120). A preliminary test in a pilot-scale processing plant achieved the frame rate up to 200 bpm (i.e. a frame rate 317 Hz). The data transfer rates (i.e. the amount of data transferred by a 3-band image per unit time) were 16 and 28 Mbps at frame rates of 286 and 500 Hz, respectively, which were much smaller than 480 Mbps of the USB 2.0 data throughput.

2.3. Hyperspectral imaging system: software

2.3.1. Carcass-image formation algorithm

A relative reflectance calibration was done at each line-scan data by a normalized difference formula, [measurement – dark current]/[99% target – dark current] (Lawrence et al., 2003b), producing values between 0 and 1 (or 0% and 99%). A 99% reflectance panel (SRT-99-120, Spectralon, North Sutton, NH, USA) was used as the white reference material. A dark current was obtained with a lens cap on the objective lens. After the reflectance calibration, a carcass-image formation algorithm was applied to create an image of each bird and spatially resolve individual surface feces on each image. The carcass-image formation algorithm acquired line scan data and determined whether the current line data belonged to a carcass or the background by monitoring reflectance values. The basic idea was to exploit the gap between birds especially between abdomens (Fig. 2). A black panel behind the shackle line made the background almost always much darker than the foreground (a carcass).

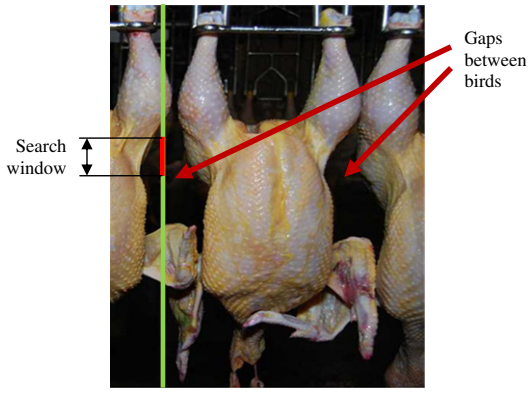

Fig. 2. Digital photo of typical birds in shackles. The hypothesis of the developed carcass detection algorithm for image formation was that there is a gap between neighboring birds such that the gap separates the birds. The search window was set along the stationary scan line.

The algorithm required to have a pre-defined set of parameters: the size of a search window and its center position along the scan line (Fig. 2). The parameters were set by the user and not changed throughout the imaging. The waveband at 517 nm was used for the carcass-image formation. The center position was set to be 40% down from the top. The search-window size was 17 pixels. The threshold value to differentiate the background (dark pixels) from the foreground (bright pixels) was 0.015, i.e. 1.5% reflectance. Now, whether the currently scanned data belonged to either a carcass or the background was determined by counting the numbers of bright and dark pixels. If there was more than one bright pixel within the search window and the immediately previous data belonged to the background, the algorithm recorded the address of the current data on a memory buffer as the start of a bird. Note that the birds moved from left to right as seen from the camera. The search for the end of the bird was just opposite. If the number of dark pixels decreased to 3 or less after recording the starting position, the algorithm recorded the current address on the memory buffer as the end of the bird. Then, the algorithm accessed the memory buffer to retrieve the data between the start and end addresses to form a carcass image. The details on how to manage the memory buffer will be explained later in the software architecture section. Before moving onto the next topic, we would like to point out that Chao et al. (2008) already developed a similar poultry carcass detection algorithm for wholesomeness inspection of poultry carcasses. However, their algorithm did not form an image of an individual bird because a region-of-interest was the basis of detection. In addition, the scan area of their algorithm was limited by not imaging thighs.

2.3.2. Fecal detection algorithm

A basic fecal detection algorithm (the basic algorithm, in short) used a band ratio of 565/517 nm followed by thresholding with a threshold 1.05 found by previous research as an optimal value. An enhanced fecal detection algorithm (the enhanced algorithm, in short) was a dual band-ratio algorithm using 565/517 and 802/517 nm and their thresholding. The enhanced algorithm performed first the basic algorithm and then another band-ratio algorithm using 802/517 nm with a threshold 1.5 again found by previous research. The second part of the enhanced algorithm was developed to remove false positive errors, especially cuticles that were not removed by the basic algorithm. Thresholding of a 517-nm image was used to create a background-mask image to suppress the background. The background-mask threshold was 0.015 (1.5% reflectance). In this research, two different studies were conducted to test the performance of the algorithms. First, three detection algorithms were compared in terms of reducing false positive errors caused by cuticles. The algorithms compared were (1) the basic algorithm with a threshold 1.05, (2) the enhanced algorithm with thresholds 1.05 and 1.5 for two band-ratios, and (3) the basic algorithm and a software cuticle removal filter with a threshold 0.4 applied to the 517-nm image. For a fair comparison, one bird was used and patched with cuticles on the carcass skin because the number of sample birds with cuticles was small. Second, the performance of the basic and enhanced algorithms was evaluated in terms of fecal detection accuracy and false positive rate at two different line speeds (140 and 180 bpm).

2.3.3. Software architecture

Fig. 3 shows the block diagram of the software architecture that consisted of user interface (UI), data acquisition, and data processing modules. The software was designed to work in the Microsoft's Visual C++ 6.0 multithreading environment such that the UI module was controlled by a UI thread, and the data acquisition and processing modules were controlled by worker threads. A UI thread handles user inputs and responds to both user and system events such as inspection start/stop, file open/save, camera and imaging

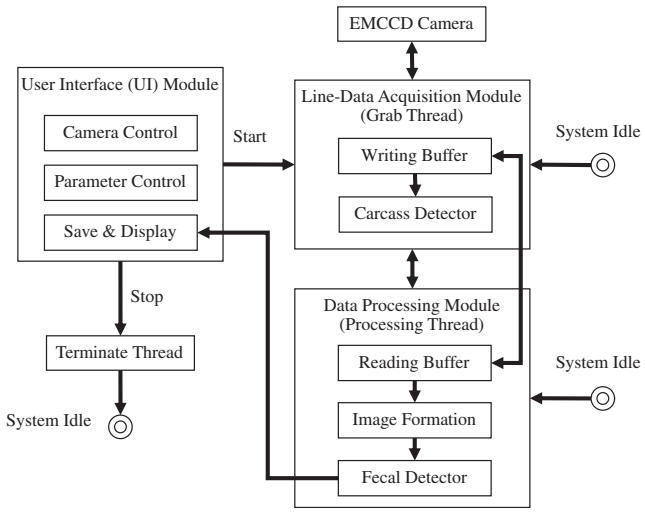

Fig. 3. Block diagram of software architecture. The UI module processes the user's request to operate the system with UI threads. The grab and processing threads are worker threads.

parameter set-ups, and image display. A worker thread handles a background task without waiting for user inputs. Thus, two worker threads were running in the background for simultaneous data acquisition and processing after acquiring the first bird image. The main function of the data acquisition module was to acquire line scan data of three wavelengths at 517, 565 and 802 nm and to store them on a circular buffer. A circular buffer (also called a ring buffer) is a data structure that uses a single, fixed-size memory buffer as if it were connected end-to-end as in a circle. When the circular buffer gets full, the buffering starts again from the beginning by overwriting the previous data. The carcass detection algorithm determined the buffer addresses corresponding to the start and end positions of a bird. The data processing module reads the line scan data on the circular buffer to form an image based on the address information obtained by the carcass detection algorithm. Finally, the fecal detection algorithm was applied to the formed image. The details of the multitasking of data acquisition and processing are described next (Fig. 4).

In C/C++ multithread programming, when concurrent processes or threads are racing each other in accessing shared resources such as memory locations, an undesired behavior called a race condition (a software defect and one of frequent software crashes) may occur. Therefore, in this research, ping-pong memory buffering (or called double buffering) was deployed in order to prevent a race condition and to speed up the execution of concurrent threads. In general, ping-pong buffering maintains two separate buffers such that one buffer receives new data while the other buffer retrieves previous data. When receiving new data is complete, the roles of two buffers are switched by swapping the pointers of the buffers. Ping-pong buffering is also popular in computer graphics for drawing graphics with no flicker and tearing. In the developed software, two identical circular buffers were used for implementing the ping-pong buffering. As in Fig. 4, at the beginning, the writing circular buffer receives new data while the reading buffer is empty. Ping-pong buffering happens when the carcass detection algorithm detects the end of a bird. As the second bird enters the field of view, the writing buffer starts receiving new data and filling the data from the position right after the last position where the previous data was filled. Simultaneously, the reading buffer starts reading the previous data from the address designated by the data acquisition module. A preliminary study found data processing after reading data from a buffer was much faster than data acquisition processing. Therefore, it was possible to complete the

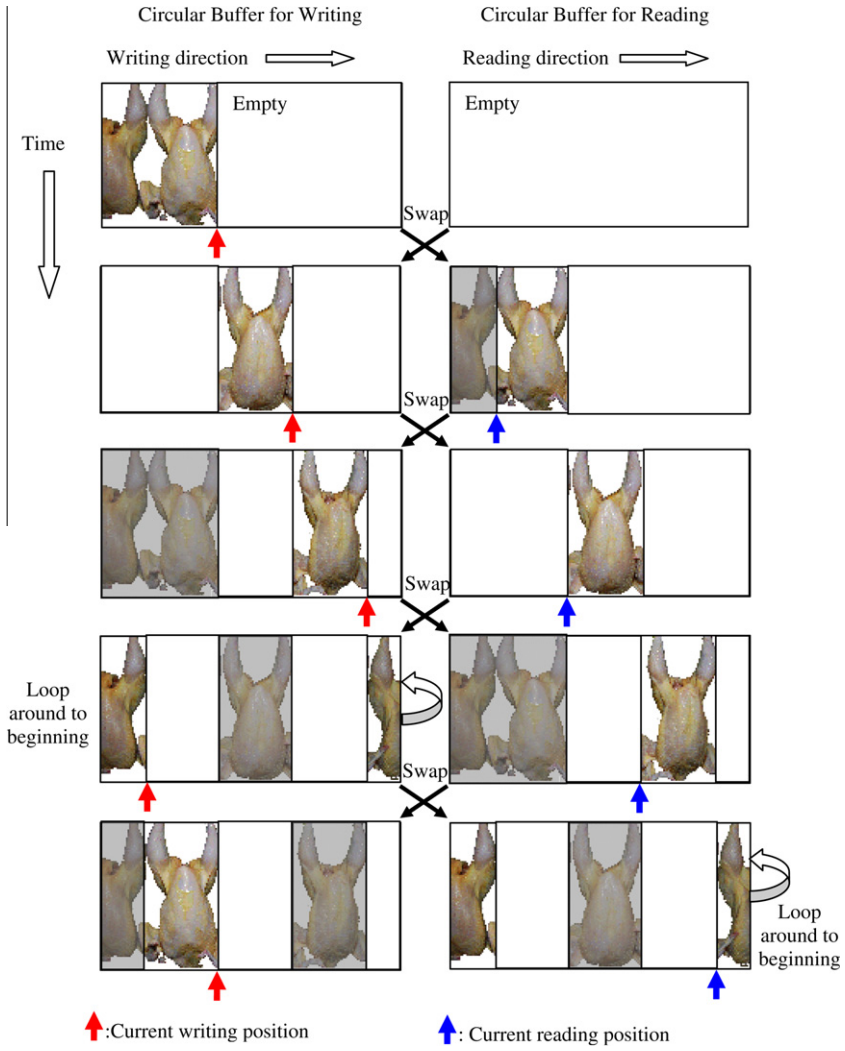

Fig. 4. Concept of writing and reading circular buffers operating ping-pong buffering. The current write/read address pointers are determined by the carcass detection algorithm.

execution of a fecal detection algorithm in real-time before the next bird comes into the field of view. As the next bird is detected, ping-pong buffering continues. When the writing buffer is full or the current reading position is at the end of the reading buffer as in the fourth and fifth rows of Fig. 4, the buffering or reading loops back to the beginning of the buffer. The grayed area in Fig. 4 designates the data of the previous birds. The ping-pong buffering continues until the user requests a stop.

There was a delay of one bird at the beginning because no acquisition happened yet. After that, the processing module processed the previous bird while the acquisition module acquired the new one. Circular memory buffers allowed an access to previous data up to about 8–10 birds while acquiring new data. The size of the circular buffer was $1004 \times 1004 \times M$, where M was the number of random tracks (i.e. 2–3 bands) and 1004 was the spatial dimension and the number of scan lines, respectively. OpenCV (a library of open source C/C++ programming functions for real time computer vision) was used for implementing basic image processing operations like median filtering.

2.4. Speed performance measurement

In order to measure the frame rates of the imaging system as a function of exposure time, the camera manufacture's software, Andor Solis was used. The following variables were considered: a trigger mode (internal or external), a random track mode (two bands or three bands). The frame transfer mode was turned on. Two random tracks (i.e. spectral bands) were selected from wavebands at 517 and 565 nm. Three tracks were selected from wavebands at 517, 565 and 802 nm. The bandwidth for the two-band case was just one track whereas the bandwidths for three bands were 13, 13, and 26 tracks centered at 517, 565 and 802 nm. The goal of this experiment was first to understand the limit of the camera's frame rate and second to find an exposure time range to be used in practice so as to meet the minimum frame rate requirement (222 Hz at 140 bpm and 286 Hz at 180 bpm). As an external trigger source, pulses generated by a 4 MHz sweep function generator (4003A, B&K Precision, Yorba Linda, CA, USA) were used for this test. The single continuous image acquisition mode was used to report the results. The actual frame rate was automatically computed by Solis and a number was read at arbitrary time because the frame rate was almost constant over time unless the user interrupted the acquisition process.

Another experiment was conducted to evaluate the speed performance of the developed software at a higher processing-line speed 200 bpm. For this experiment, the developed fecal detection software was used for image grabbing and processing in the described multitasking environment. Both image grab time and

process time were measured and recorded in a text output file. The grabbing time refers to the time for which the software grabbing module spent to form a 3D data cube of the dimension N (width) $\times$ 512 (height) $\times$ 3 (bands/tracks), where N was 128 and 118 scans per bird. If the software grabbed more than 95 lines per bird and processed them within 300 ms simultaneously, it implied that the software would meet the minimum speed requirement at 200 bpm. A white foam board was used as a target. The software continuously ran for 1 h. The number of 3D data cube files created and saved was 12,078 for 1 h which was equivalent to the data amount generated by the speed 201 bpm.

2.5. Imaging protocol and bird samples

Fresh 16 chicken carcasses were obtained from a local poultry processing plant and used for testing the developed imaging system. Four chicken carcasses were obtained before the washer in the processing plant. They had cuticles on their bodies. Therefore, they were used to study cuticle effects (i.e. false positive errors). The rest 12 chicken carcasses were obtained after the washer in order to test the system performance. The developed imaging system was tested under two different processing line speeds (140 and 180 bpm) in a pilot-scale processing plant at the Russell Research Center, Athens, GA, USA. Three types of fecal materials (duodenum, ceca, and colon) and digestive matter (ingesta) obtained from the sample birds were pasted on each of 12 carcasses for evaluation of the detection algorithms. It was attempted to paste each of four fecal materials at one random spot per bird (Fig. 5 as an example). But, it was very difficult to paste each material at one single location without being smeared because most fecal materials were mushy. Some of fecal materials were dropped from the shackle motion or washed out due to excessive moisture or water on the carcass surfaces because mist water was sprayed in order to produce environment conditions similar to those in poultry processing plants. Especially, the duodenum materials were yellowish runny droppings. Therefore, the exact amount of each paste was not measured and the size of each spot with contiguous pixels varied from a few pixels to about 150 pixels. Clean birds were imaged first and then fecal materials were applied onto the clean birds before imaging them as dirty birds. As in Fig. 5(c), regions-of-interest (ROI) were manually obtained as ground-truth data for data analysis and used for evaluating the performance of fecal detection algorithms.

3. Results and discussions

3.1. Speed performance

As shown in Fig. 6, it was found that any exposure time shorter than 100 μs exceeded the minimum frame rate requirement (>222 Hz). The results of external triggering suggested the faster frame rate than internal triggering. Also, astute readers may suggest that the minimum frame rate requirement 286 Hz for the faster line speed like 180 bpm may not be met if internal triggering is used. Note that no spatial binning was used for this test. If 1 $\times$ 2 spatial binning was used, it was expected to achieve the frame rate 286 Hz.

The grabbing time of the application software for 128 lines was greater than 300 ms. Thus, there was a delay in grabbing so that a race condition could occur and cause incorrect and unexpected results. On the other hand, it was found that grabbing 118 lines per bird met the minimum requirement. The grabbing time was 282 ms for 118 scans. In this case, the processing time was approximately in between 47 and 86 ms. This simulation suggested that plenty of processing time (more than extra 200 ms) could be assigned to other tasks. Thus, the bottleneck of the imaging system was the data acquisition. The CPU usage was approximately 6–11%. The memory usage was 92 KB without any software issues such as memory leaks. In conclusion, the software could handle the 200-bpm processing speed while producing high resolution images with 118 (width) $\times$ 512 (height) $\times$ 3 (bands) resolution.

3.2. Performance of algorithms for removing cuticles

The test results of the aforementioned three algorithms are presented in Fig. 7 and Table 1 to show their cuticle-removal performance. The enhanced algorithm using three bands almost completely removed the cuticle pixels from the false positive errors detected by the basic algorithm (only two pixels left). The software cuticle filter also removed most of cuticle pixels except edge pixels that were darker than inner pixels. Most false positives (red) except cuticle pixels (cyan) were found along edges of a carcass body and were isolated pixels. These isolated pixels along the body boundaries were be easily removed by morphological erosion. False positives of inner pixels were small and isolated so that median filtering can be used to remove them in practice. It was found that optical density of cuticles mattered most in addition to their

Fig. 5. Pictures of a test bird with surface fecal materials: (a) taken by a digital camera, (b) taken and constructed by the imaging system to display it in pseudo-color using three wavebands, and (c) regions-of-interest (ROI) were manually created for feces (red) and normal skins (green). (For interpretation of the references to color in this figure legend, the reader is referred to the web version of this article.)

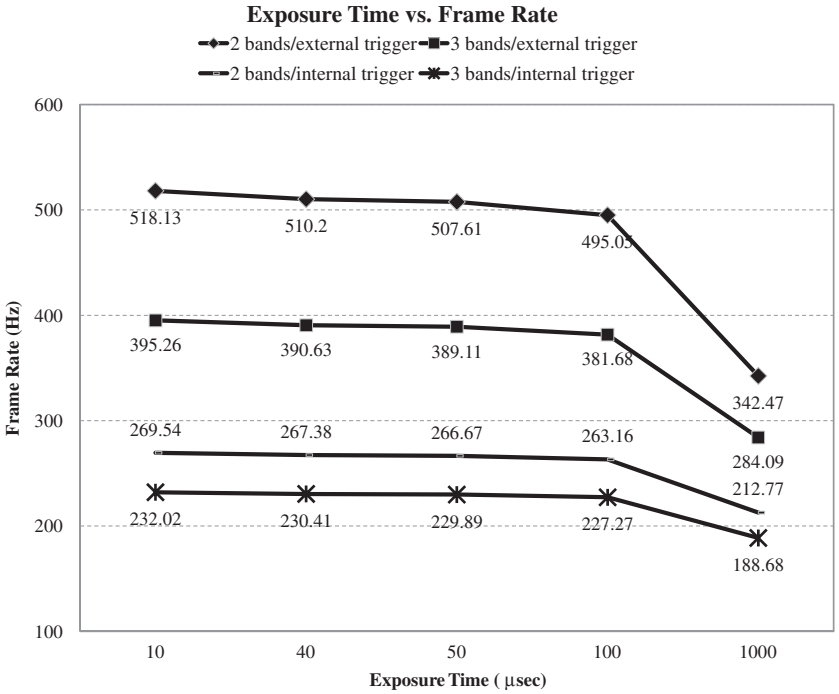

Fig. 6. Exposure time and frame rate.

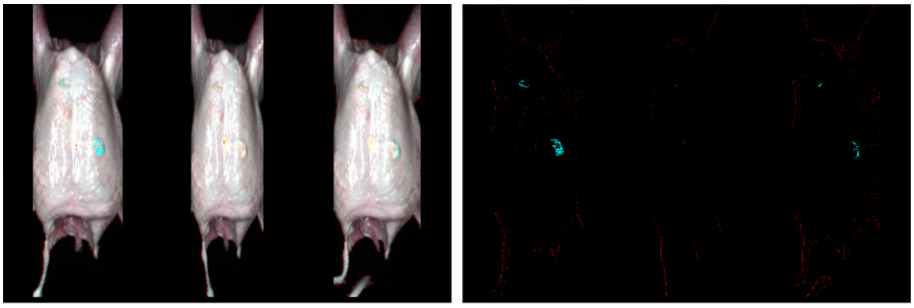

Fig. 7. Comparision of three detection algorithms using 2 bands (basic), 3 bands (enhanced), and 2 bands with software cuticle filtering (basic with a software filter) from the left to the right, respectively. The cyan color pixels were false positives due to cuticles. The red color pixels were the rest of the false positives. (For interpretation of the references to color in this figure legend, the reader is referred to the web version of this article.)

Table 1
Comparison of three detection algorithms in terms of cuticle removal performance.

	All false positives (pixels)	Cuticles (pixels)	Cuticles among all false positives (%)
Basic alg.	575	225	39.1
Enhanced alg.	154	2	1.3
Basic alg. w/a cuticle filter	517	66	12.8

sizes. The thicker the cuticles are, the more the false positives are. In conclusion, the enhanced algorithm was the best in removing cuticles (~100% with post-processing filtering). The enhanced algorithm also reduced about 73% of false positive error pixels from 575 pixels to 154 pixels. So far, the spatial distribution of cuticles and false positives was discussed.

Next, data distribution patterns visualized by scatter plots were studied to learn distribution patterns of cuticles and false positives. From the same data used in Fig. 7, cuticle pixels ($N = 293$) and other false positive pixels ($N = 953$) were divided into two groups. Fig. 8 shows a scatter plot of these two groups seen at the axes of wavelengths 517 and 802 nm. As shown in the figure, cuticles and most false positives were effectively removed by the decision boundary determined by 1.5. The red cuticle pixels were distributed relatively evenly from 0.35 to 0.5. However, the dark pixels below 0.15 shown at 517 nm were still not removed by the decision boundary. Most of these dark false positive pixels were mixed pixels of background and body contours. Erosion of bird mask image must be an effective solution to deal with the contour problem. Alternatively, a new decision boundary (piecewise linear) by adding a line as shown in Fig. 8 and median filtering can be also considered as a method to remove the remaining false positives.

3.3. Performance of fecal detection algorithm

Fig. 9 shows a mosaic of pseudo-color composite images made from 3-wavebands obtained by the system (see also Fig. 5(b) to zoom in the fifth image on the first row). The 12 different birds were used to study the efficacy of the fecal detection algorithms (basic and enhanced). The following system parameters were used

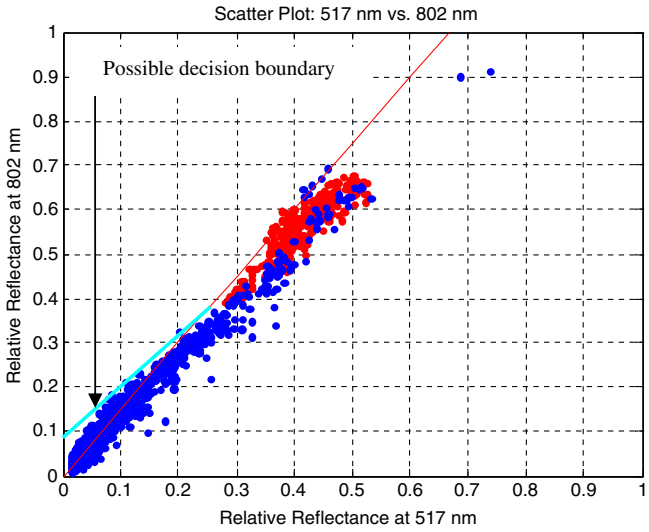

Fig. 8. 2D scatter plot of false positives in Fig. 7 as seen from the 517- and 802-nm space. The red line was a decision boundary determined by the threshold 1.5. The red pixels were cuticles. The blue pixels were the remaining false positives. (For interpretation of the references to color in this figure legend, the reader is referred to the web version of this article.)

to construct three-waveband images with 118 (width) × 512 (height) × 3 (bands) pixels. The exposure time was 1.68 ms. The EM gain of the EMCCD camera was 4. The bandwidths of three wavebands were 13 at 517 nm, 9 at 56 nm and 21 at 802 nm. The top-row images of Fig. 9 were obtained at 140-bpm whereas the bottom images were obtained at 180 bpm. Thus, the differences in bird widths were caused mainly by different shackle-line speeds. The overall system operation with real birds in a pilot-scale processing plant was also examined by running the line over an hour. The carcass detection algorithm worked as designed. The speed of the software met the minimum requirement. The number of ROI spots obtained from the images in Fig. 9 were 113 (58 and 55 at 140 and 180 bpm, respectively). Thus, the higher speed (180 bpm) missed three small spots that were captured at 140 bpm. The average size of each ROI was 37 and 28 pixels at 140 and 180 bpm, respectively. The minimum ROI size was 1 at both speeds. The maximum ROI sizes were 151 and 98 pixels at 140 and 180 bpm, respectively. The ROI size of fecal materials was 3710 pixels (2159 and 1551 pixels at 140 and 180 bpm, respectively). Again, the 180-bpm speed captured the less number of fecal pixels than 140 bpm. Table 2 quantitatively summarizes

Table 2
Comparison of two detection algorithms in terms of fecal detection accuracy at two line speeds.

Algorithm	Line speed (bpm)	Post-processing (3 × 3 median filtering)	False negatives	False positives
Basic	140	No	10.6% (N = 229)	0.3% (N = 1191)
Enhanced	140	No	9.2% (N = 199)	0.1% (N = 405)
Basic	140	Yes	1.1% (N = 24)	∼0% (N = 3)
Enhanced	140	Yes	4.9% (N = 106)	0% (N = 0)
Basic	180	No	11.0% (N = 171)	0.3% (N = 940)
Enhanced	180	No	8.8% (N = 137)	0.1% (N = 334)
Basic	180	Yes	1.8% (N = 26)	0% (N = 0)
Enhanced	180	Yes	4.1% (N = 64)	0% (N = 0)

the performance of the basic and enhanced algorithms in terms of false positive and false negatives (missed feces) at the pixel level. First, the detection algorithms detected ROI fecal pixels with the accuracy ranging from 89% (basic, no median filtering, 180 bpm) to 98% (basic, median filtering, 140 bpm). The false positive rates were less than 0.4% in all cases. The performance difference between two speeds at 140 and 180 bpm was very small. The system at 180 bpm could not image some pixels that otherwise would be captured at 140 bpm. Those pixels captured at 140 bpm still may or may have not been detected. The qualitative evaluation at the blob level found no ROI blobs of feces were missed in all cases. However, this research finding suggested the real future challenge would be detecting small fecal spots at 180 bpm or faster. This top is an important question for future research.

Fig. 10 shows 2D scatter plots of the ROI obtained from Figs. 8 and 9. The data in the ROI were based on two wavelength combinations (i.e. 517 versus 565 nm and 517 versus 802 nm). Also, the ROI used for cuticle-skin distribution analysis were added to the ROI data set for Fig. 10(a) and (b). The scatter plots in Fig. 10(c) and (d) were obtained from the ROI pixels after a 3 × 3 morphological erosion filter was applied to the ROI pixels in Fig. 10(a) and (b). All pixels above the lines in the scatter plots were feces candidates where in fact, false positives were included especially in Fig. 10(a) and (b). The obvious false positives removed in Fig. 10(c) and (d) were cuticles and dark pixels with reflectance values less than 0.2. As shown in Fig. 10(c) and (d), the morphological erosion removed false positives as well as true fecal pixels. This result quantitatively confirmed the previous observation that most of the false positives other than cuticles were at the boundaries of true feces ROI. Due to the nature of the erosion operation, most of removed pixels along the fecal ROI boundaries were spectrally mixed. In

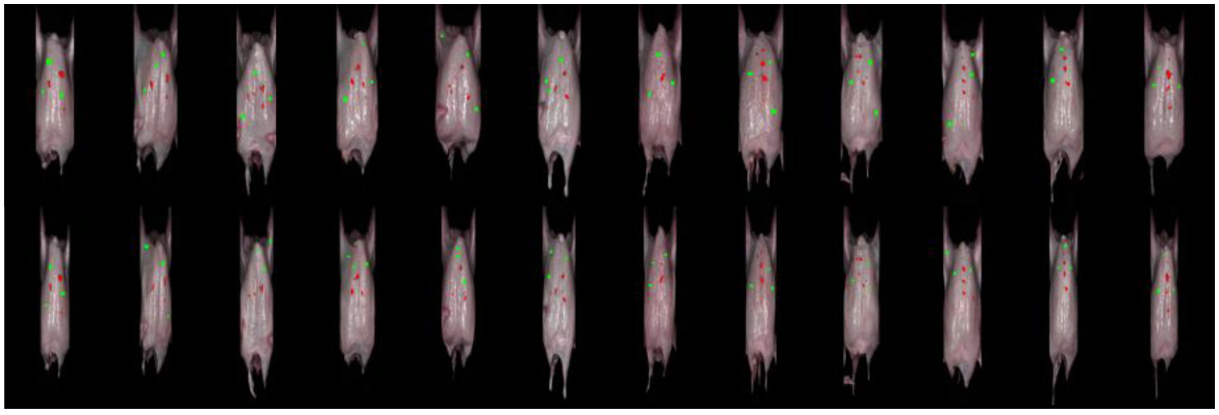

Fig. 9. Mosaic of dirty birds contaminated by fecal materials: ROI (red: feces and green: normal skin). The top row includes the images taken 140 bpm and the bottom row includes the images taken at 180 bpm. (For interpretation of the references to color in this figure legend, the reader is referred to the web version of this article.)

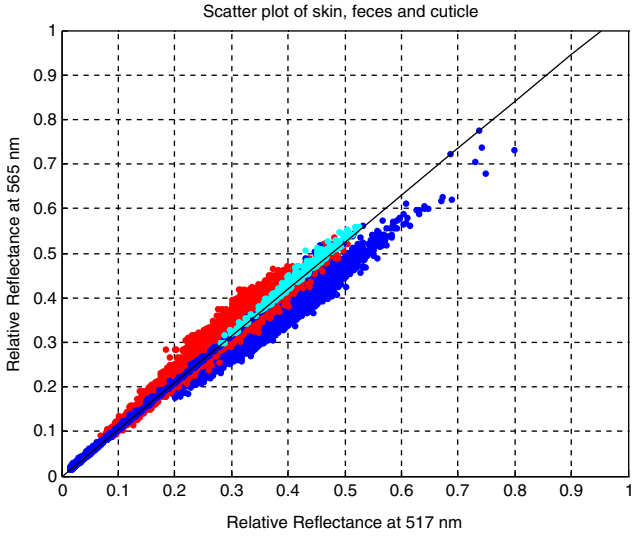

(a) 517 nm vs 565 nm

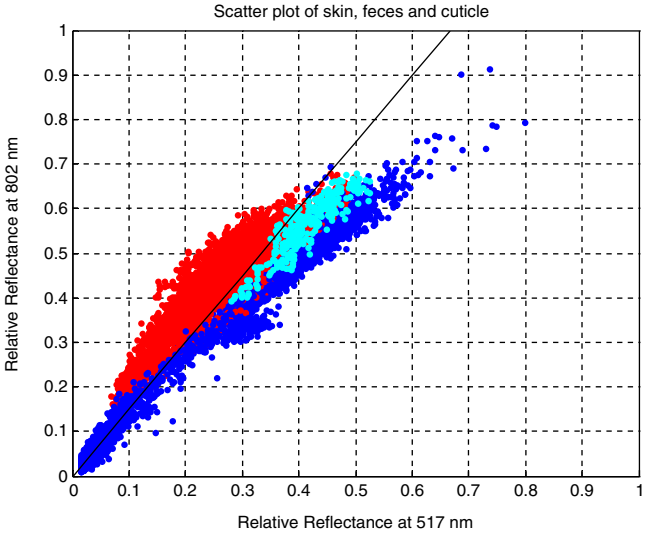

(b) 517 nm vs 802 nm

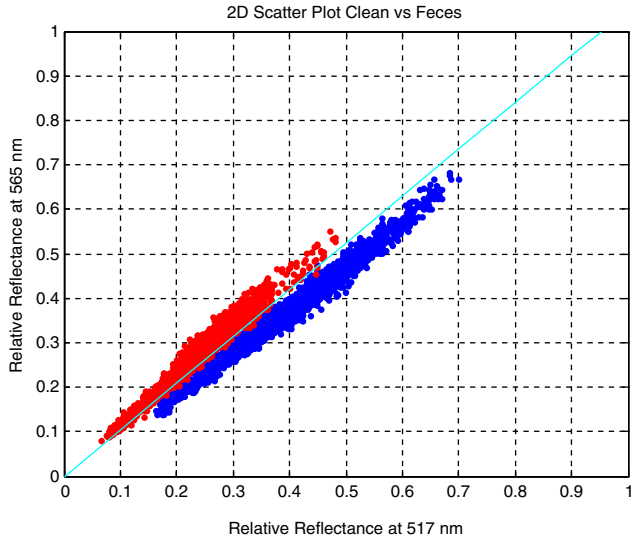

(c) Eroded ROIs: 517 nm vs 565 nm

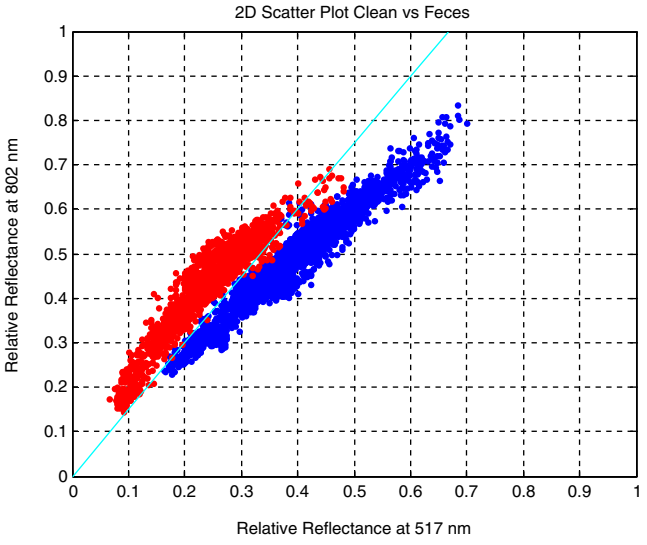

(d) Eroded ROIs: 517 nm vs 802 nm

Fig. 10. Scatter plots of normal skin (blue), feces (red) and cuticles (cyan). Decision boundaries (line) were overlaid with band-ratio thresholds (a) 1.05 and (b) 1.5. The scatter plots in (c) and (d) were obtained from the ROI after being filtered by a 3×3 morphological erosion. (For interpretation of the references to color in this figure legend, the reader is referred to the web version of this article.)

summary, the study on the advanced fecal detection algorithm using the three bands found that the cuticles and the feces were well separable by thresholding the ratio of 802 and 517 nm with the threshold value 1.5. This finding was also consistent with the previous study. But, when the pixels were linked to optically less opaque feces like duodenums or small size feces, the advanced fecal detection algorithm may also remove mixed pixels around feces. Thus, boundary pixels of small fecal spots were prone to the thresholding operation of the second band-ratio algorithm using 802 nm because median filtering possibly wipes out the leftovers in practice.

4. Conclusions

The real-time fecal detection with the developed line-scan hyperspectral imaging system was possible due to (1) data binning utilizing the unique feature of the EMCCD sensor (a random track mode) that was capable of getting access to user-defined areas on the CCD sensor and (2) the design of the custom software supporting multitasking. The speed test of the designed line-scan hyperspectral imaging system demonstrated a commercialization potential of the system. The fecal detection algorithms using 517, 565 and 802 nm confirmed the efficacy of the fecal detection while minimizing the chance of falsely identified chicken carcasses. The performance of fecal detection was comparable to what the previous research achieved. The study suggested that the real-time multispectral imaging using a hyperspectral image camera could be also feasible in other applications.

Acknowledgements

The authors would like to express a deep appreciation to Allan Savage and Peggy Feldner for their support and help for this project.

References

Berrang, M.E., Smith, D.P., Windham, W.R., Feldner, P.W., 2004. Effect of intestinal content contamination on broiler carcass *Campylobacter* counts. Journal of Food Protection 67 (2), 235–238.

Chao, K., Yang, C.C., Kim, M.S., Chan, D.E., 2008. High throughput spectral imaging system for wholesomeness inspection of chicken. Applied Engineering in Agriculture 24 (4), 475–485.

Chao, K., Yang, C.-C., Chen, Y.-R., Kim, M.S., Chan, D.E., 2007. Hyperspectral-multispectral line-scan imaging system for automated poultry carcass inspection applications for food safety. Poultry Science 86 (11), 2450–2460.

FSIS, USDA, 1998a. HACCP-based inspection models project: diseases and conditions observable in meat and poultry. Available online at: <http://www.fsis.usda.gov> (accessed 20.08.2011).

FSIS, USDA, 1998b. FSIS clarifies and strengthens enforcement of zero tolerance standard for visible fecal contamination of poultry. Available online at: <http://www.fsis.usda.gov> (accessed 20.08.2011).

FSIS, USDA, 2004. HACCP-based inspection models project (HIMP): young chicken inspection. Available online at: <http://www.fsis.usda.gov> (accessed 20.08.2011).

Grietens, B., 2009. InGaAs cameras allow broader NIR applications. Optics & Laser Europe. Available online at: <http://www.xenics.com> (accessed 20.08.2011).

Heitschmidt, G.W., Park, B., Lawrence, K.C., Windham, W.R., Smith, D.P., 2007. Improved hyperspectral imaging system for fecal detection on poultry carcasses. Transaction of the ASABE 50 (4), 1427–1432.

Kehtarnavaz, N., Gamadia, M., 2006. Real-Time Image and Video Processing: from Research to Reality. Morgan & Claypool, San Rafael, CA.

Kim, M.S., Lee, K., Chao, K., Lefcourt, A.M., Jun, W., Chan, D.E., 2008. Multispectral line-scan imaging system for simultaneous fluorescence and reflectance measurements of apples: multitask apple inspection system. Sensing and Instrumentation for Food Quality and Safety 2 (2), 123–129.

Lawrence, K.C., Windham, W.R., Park, B., Buhr, R.J., 2003a. A hyperspectral imaging system for identification of fecal and ingesta contamination on poultry carcasses. Journal of Near Infrared Spectroscopy 11 (4), 269–281.

Lawrence, K.C., Park, B., Windham, W.R., Mao, C., 2003b. Calibration of a pushbroom hyperspectral imaging system for agricultural inspection. Transaction of the ASAE 46 (2), 513–521.

Leitner, R., Mairer, H., Kercek, A., 2003. Real-time classification of polymers with NIR spectral imaging and blob analysis. Real-Time Imaging 9 (4), 245–251.

Litwiller, D., 2001. CCD vs. CMOS: facts and fiction. Photonics Spectra 35 (1), 154–158.

Litwiller, D., 2005. CCD vs. CMOS: maturing technologies, maturing markets. Photonics Spectra 39 (8), 54–61.

Park, B., Lawrence, K.C., Windham, W.R., Buhr, R.J., 2002. Hyperspectral imaging for detecting fecal and ingesta contaminants on poultry carcasses. Transaction of the ASAE 45 (6), 2017–2026.

Park, B., Lawrence, K.C., Windham, W.R., Smith, D.P., 2004. Multispectral imaging system for fecal and ingesta detection on poultry carcasses. Journal of Food Process Engineering 27, 311–327.

Park, B., Kise, M., Lawrence, K.C., Windham, W.R., Smith, D.P., Thai, C.H., 2007. Real-time multispectral imaging system for online poultry fecal inspection using unified modeling language. Sensing and Instrumentation for Journal of Food Quality and Safety 1 (2), 45–54.

Park, B., Yoon, S.C., Windham, W.R., Lawrence, K.C., Heitschmidt, G.W., Kim, M., Chao, K., 2011. Line-scan hyperspectral imaging for real-time on-line poultry fecal detection. Sensing and Instrumentation for Journal of Food Quality and Safety 5 (1), 25–32.

Tatzer, P., Wolf, M., Panner, T., 2005. Industrial application for inline material sorting using hyperspectral imaging in the NIR range. Real-Time Imaging 11 (2), 99–107.

Windham, W.R., Lawrence, K.C., Park, B., Buhr, R.J., 2003a. Visible/NIR spectroscopy for characterizing fecal contamination of chicken carcasses. Transaction of the ASAE 46 (3), 747–751.

Windham, W.R., Smith, D.P., Park, B., Lawrence, K.C., Feldner, P.W., 2003b. Algorithm development with visible-near-infrared spectral for detection of poultry feces and ingesta. Transaction of the ASAE 46 (6), 1733–1738.

Yoon, S.C., Lawrence, K.C., Park, B., Windham, W.R., 2007. Statistical model-based thresholding of multispectral images for fecal detection on poultry carcasses. Transaction of the ASABE 50 (4), 1433–1442.

Yoon, S.C., Park, B., Lawrence, K.C., Windham, W.R., and Heitschmidt, G.W., 2010. Development of real-time line-scan hyperspectral imaging system for online agricultural and food product inspection. Sensing for Agriculture and Food Quality and Safety II. Proc. SPIE, vol. 7676.